non peer-reviewed preprint submitted to PNAS

Functional relationships reveal differences in the water cycle representation of global water models

Sebastian J. Gnann[a,*], Robert Reinecke[a], Lina Stein[a], Yoshihide Wada[b,c], Wim Thiery[d], Hannes Müller Schmied[e,f], Yusuke Satoh[g], Yadu Pokhrel[h], Sebastian Ostberg[i], Aristeidis Koutroulis[j], Naota Hanasaki[k], Manolis Grillakis[j], Simon N. Gosling[l], Peter Burek[c], Marc F. P. Bierkens[m,n], and Thorsten Wagener[a]

[a]Institute of Environmental Science and Geography, University of Potsdam, Potsdam, Germany

[b]Climate and Livability, Biological and Environmental Science and Engineering Division, King Abdullah University of Science and Technology, Thuwal, Saudi Arabia

[c]International Institute for Applied Systems Analysis, Laxenburg, Austria

[d]Department of Hydrology and Hydraulic Engineering, Vrije Universiteit Brussel, Brussels, Belgium

[e]Institute of Physical Geography, Goethe University Frankfurt, Frankfurt am Main, Germany

[f]Senckenberg Leibniz Biodiversity and Climate Research Centre (SBiK-F), Frankfurt am Main, Germany

[g]Moon Soul Graduate School of Future Strategy, Korea Advanced Institute of Science and Technology, Korea

[h]Department of Civil and Environmental Engineering, Michigan State University, East Lansing, MI, USA

[i]Potsdam Institute for Climate Impact Research (PIK), Member of the Leibniz Association, Potsdam, Germany

[j]School of Chemical and Environmental Engineering, Technical University of Crete, Greece

[k]National Institute for Environmental Studies, Tsukuba, Japan

[l]School of Geography, University of Nottingham, Nottingham, United Kingdom

[m]Department of Physical Geography, Utrecht University, The Netherlands

[n]Unit Soil and Groundwater Systems, Deltares, Utrecht, The Netherlands

*Correspondence: gnann1@uni-potsdam.de

Functional relationships reveal differences in the water cycle representation of global water models

Sebastian J. Gnann[a,1,2], **Robert Reinecke**[a,1], **Lina Stein**[a], **Yoshihide Wada**[b,c], **Wim Thiery**[d], **Hannes Müller Schmied**[e,f], **Yusuke Satoh**[g], **Yadu Pokhrel**[h], **Sebastian Ostberg**[i], **Aristeidis Koutroulis**[j], **Naota Hanasaki**[k], **Manolis Grillakis**[j], **Simon N. Gosling**[l], **Peter Burek**[c], **Marc F. P. Bierkens**[m,n], **and Thorsten Wagener**[a]

[a]Institute of Environmental Science and Geography, University of Potsdam, Potsdam, Germany; [b]Climate and Livability, Biological and Environmental Science and Engineering Division, King Abdullah University of Science and Technology, Thuwal, Saudi Arabia; [c]International Institute for Applied Systems Analysis, Laxenburg, Austria; [d]Department of Hydrology and Hydraulic Engineering, Vrije Universiteit Brussel, Brussels, Belgium; [e]Institute of Physical Geography, Goethe University Frankfurt, Frankfurt am Main, Germany; [f]Senckenberg Leibniz Biodiversity and Climate Research Centre (SBiK-F), Frankfurt am Main, Germany; [g]Moon Soul Graduate School of Future Strategy, Korea Advanced Institute of Science and Technology, Korea; [h]Department of Civil and Environmental Engineering, Michigan State University, East Lansing, MI, USA; [i]Potsdam Institute for Climate Impact Research (PIK), Member of the Leibniz Association, Potsdam, Germany; [j]School of Chemical and Environmental Engineering, Technical University of Crete, Greece; [k]National Institute for Environmental Studies, Tsukuba, Japan; [l]School of Geography, University of Nottingham, Nottingham, United Kingdom; [m]Department of Physical Geography, Utrecht University, The Netherlands; [n]Unit Soil and Groundwater Systems, Deltares, Utrecht, The Netherlands

This manuscript was compiled on December 2, 2022

Global water models are widely used for policy-making and in scientific studies, but substantial inter-model differences highlight the need for additional evaluation. Here we evaluate global water models by assessing so-called functional relationships between system forcing and response variables. The more widely used comparisons between observed and simulated fluxes provide insight into model behavior for the representative area of an observation, and can therefore potentially improve the model for that area. Functional relationships, by contrast, aim to capture how system forcing and response variables co-vary across large scales, and thus offer the potential for model improvement over large areas. Using 30-year annual averages from 8 global water models, we quantify such functional relationships by calculating correlations between key forcing variables (precipitation, net radiation) and water fluxes (actual evapotranspiration, groundwater recharge, total runoff). We find strong disagreement for groundwater recharge, some disagreement for total runoff, and the best agreement for evapotranspiration. Observation- and theory-derived functional relationships show varying agreements with models, indicating where model representations and our process understanding are particularly uncertain. Overall, our results suggest that model improvement is most important for the representation of energy balance processes, recharge processes, and generally for model behavior in dry and cold regions. We argue that advancing our ability to simulate global hydrology requires a better perceptual understanding of the global water cycle. To evaluate if our models match that understanding, we should explore alternative evaluation strategies, such as the use of functional relationships.

global hydrological models | land surface models | model evaluation | rank correlations | global hydrology

Global water models – including hydrological, land surface, and dynamic vegetation models (1) – inform water management policies. Many global modeling studies explicitly aim to provide policy-relevant information (e.g. 2–6). The Sixth Assessment Report (AR6) of the Intergovernmental Panel on Climate Change (IPCC) (7) draws heavily on results from global water models, which provide information on the impacts of climate change on streamflow (8, 9), terrestrial water storage (10), and groundwater recharge (11). Some of these models are embedded in global water information services to provide water information to a wide array of stakeholders. For instance, the Global Groundwater Information System (12) shares information required for sustainable groundwater resources development and management. The Aqueduct framework (13) calculates risk indicators to derive water risk maps valuable for companies, governments, and non-governmental organizations. And the African Flood and Drought Monitor (14) continuously predicts drought and flood indicators using various forecasting products.

Global water models have also become an essential tool in Earth system science. Measurements of some hydrological variables are very sparse and insufficient for large-scale analyses. Hence we regularly use global water models to provide globally coherent estimates of variables such as groundwater recharge and groundwater storage change (15–17). These model outputs are often the basis for other studies, e.g. by providing groundwater recharge as input to groundwater models (e.g.

Significance Statement

Global water models inform water management policies and are a cornerstone of Earth system science. Since global water models are increasingly used for projections of environmental change impacts, adequate methods to evaluate these models are imperative. Here we evaluate model behavior by comparing large-scale functional relationships between system drivers (climate forcing) and simulated and observed system outputs (water fluxes). We find substantial variability between models, and disagreements with observation-based functional relationships. For example, some models show a very strong relationship between groundwater recharge and precipitation, while others do not. Thus, projected changes in precipitation would result in different groundwater recharge estimates across models. Existing disagreements underscore the need for adequate evaluation strategies and for multi-model approaches to embrace uncertainty.

[1]S.J.G. contributed equally to this work with R.R.

[2]To whom correspondence should be addressed. E-mail: gnann1@uni-potsdam.de

18, 19), making subsequent study results dependent on the reliability of model outputs. Global models also provide a virtual laboratory which is used to assess the impacts of climate and land use change on the water cycle and on hydrological extremes such as floods and droughts (e.g. 8, 9, 20, 21).

Model disagreements highlight the need for model evaluation. Past studies have revealed substantial disagreements between global water models, showing that estimates of both the current distribution and future trends of key water cycle components remain uncertain (11, 22–25). While some of that uncertainty stems from projected or observed climatic forcing, considerable uncertainty stems from global water models themselves (8, 11, 22, 23, 26, 27). For instance, Beck et al. (23) found distinct inter-model performance differences when comparing simulated and observed streamflow for 10 global water models driven by the same meteorological forcing. Comparing long-term trends in modeled terrestrial water storage to GRACE satellites, Scanlon et al. (24) found that global models generally underestimate trends and even show opposite trends in some parts of the world. Different system conceptualizations, such as including karst-related subsurface heterogeneity, can lead to very different groundwater recharge estimates for current and potential future climates (28). It is therefore not surprising that the IPCC's AR6 (7) concludes from an analysis of currently available global water model projections that "uncertainty in future water availability contributes to the policy challenges for adaptation, for example, for managing risks of water scarcity".

To address inter-model differences as a source of uncertainty, it is imperative that we evaluate how, where and why models differ. Evaluating global models is, however, challenging due to limitations in data availability (spatial and temporal bias, data quality) and scale mismatches between observations and model outputs (29). These challenges are not easy to overcome, but they should motivate us to seek model evaluation strategies that are suitable for global water models and better utilize the information contained in the observations we have.

Towards functional model evaluation. Most evaluation strategies compare model outputs to historical observations over the footprint for which the observation is representative. This can be at the plot (e.g. flux towers), the catchment (e.g. gauging stations), or grid cell (e.g. gridded remote sensing products) scale. Such approaches are necessary but not sufficient to robustly evaluate global models (29). First, these approaches compare simulated and observed values location by location (or catchment by catchment), even though observations in one location might contain information about geographically different, but hydrologically similar, locations. Thus we might miss the opportunity to improve the model for more than one location at a time. Second, relevant information for model evaluation might not just lie in comparing the magnitudes of simulated and observed values of a variable at a single location, but rather in how a model simulates the spatial distribution of a variable (i.e. its relative differences). And third, a comparison with historical observations does not guarantee that a model reliably predicts system behavior under changing conditions (30). We think that an alternative approach can at least partially overcome these three shortcomings.

In this alternative strategy, we focus on the effective functional behavior of models (31). Effective functional behavior might be characterized by the relationship between system forcing and response variables. For example, the concept of equilibrium climate sensitivity, which quantifies the warming response to doubling carbon dioxide concentrations, is often used to describe how severe climate change might be (32). In hydrology, the sensitivity (or elasticity) of streamflow to changing climatic boundary conditions (33, 34) has been used to better understand how changes in forcing translate into changes in streamflow. This sensitivity can be used as an indicator of how quickly future water availability might change under a changing climate (35). Forcing-response relationships like these might be derived from (or constrained by) observations and theory, but also by expert knowledge, thus enabling us to bring our perception of how a system functions into the model evaluation process (36).

Here we use so-called functional relationships and explore their potential for global water model evaluation. We define the term functional relationship as a relationship between two (or more) variables, such as forcing-response relationships, or relationships between system states and fluxes. Ideally, such relationships should be based on process knowledge and first principles, but empirical relationships may serve as a useful starting point. Functional relationships have been used, for example, to analyze land surface model functioning (31), to evaluate catchment models (37), to derive constraints for model regionalization (38), or to calibrate large-scale hydrological models (39, 40). These examples are, however, scattered among the literature and have not yet been formalized into an evaluation framework. In the following, we outline how an evaluation using functional relationships might look like, show how it can help to shed new light on model behavior, and discuss next steps required to fully benefit from functional relationship based evaluation.

We evaluate 8 global water models (CLM4.5 (41), CWatM (42), H08 (43), JULES-W1 (44), LPJmL (45), MATSIRO (46), PCR-GLOBWB (47), and WaterGAP2 (48)) from phase 2b of the Inter-Sectoral Impact Model Intercomparison Project (ISIMIP 2b; 49). We analyze 30-year (climatological) averages (1975-2004) using HadGEM2-ES forcing; note that the specific forcing chosen does not appear to influence model-based functional relationships (see Materials and Methods section). We analyze the following model variables: precipitation P (the available water; equal for all models), net radiation N (a proxy for the available energy), actual evapotranspiration E_a, groundwater recharge R, and total runoff Q (three key water fluxes), all converted to mm/y. Details on data processing are described in the Materials and Methods section.

We address the following three research questions:

1) To what extent do key water fluxes simulated by global water models disagree with each other, and how does the disagreement vary spatially?
2) How do global water models translate forcing variables into key water fluxes, i.e. which functional relationships do they represent?
3) Can we use data and existing knowledge to derive functional relationships and use them to constrain expected model behavior?

Results

Research question 1: Global model disagreement. We first assess how model outputs (actual evapotranspiration, groundwater recharge, total runoff) vary globally by calculating the coefficient of variation (CoV) between the 8 models per grid cell, shown in Figure 1a-c (see Materials and Methods for details). Actual evapotranspiration (Figure 1a) shows low CoV values suggesting reasonable agreement between models (mean grid cell CoV = 0.23), with slightly higher CoV values in some mountainous regions (e.g. Himalaya) and cold regions (e.g. northern Russia). Groundwater recharge (Figure 1b) shows many white spaces suggesting strong disagreement (mean grid cell CoV = 1.17). The highest CoV values are found in dry regions (e.g. Australia, outer-tropical Africa) and in cold regions (e.g. large parts of continental Asia and North America). Total runoff (Figure 1c) shows some white spaces suggesting moderate disagreement (mean grid cell CoV = 0.54). The highest CoV values are found in dry regions (e.g. Australia, outer-tropical Africa, Central Asia). Note that the CoV can be high even if the absolute differences are small, so that inter-model differences might be exaggerated in very dry regions. We thus show maps of the standard deviation in the Supporting Information (Figures S5-7).

When exploring inter-model differences, it is useful to assess if strong model disagreement (high CoV values) is due to high ensemble uncertainty (all models disagree with each other) or because one individual model deviates strongly. Figure 1d-f shows which model deviates most from the ensemble mean, indicating which model dominates the ensemble spread (i.e. the CoV shown in Figure 1a-c). While this does not tell us which models perform better or worse, it indicates whether there is a single model that is consistently different (in a certain region). We find that different models deviate from the ensemble mean in different places. There is not one model that consistently deviates the most for a specific variable (the highest fraction of grid cells dominated by a single model for E_a, R, and Q, is 12%, 14%, and 13%, respectively), but mostly multiple models deviate similarly strongly from the ensemble mean (for E_a, R, and Q, it is 31%, 28%, and 34%, respectively). Overall, there is little agreement between the maps and we cannot single out one model that consistently deviates the most for all fluxes over a large region (Figures 1d-f show different patterns).

Research questions 2 and 3: Functional relationships. We can visually assess relationships between forcing (P, N) and response variables (E_a, R, Q) by inspecting scatter plots, exemplarily shown for some variable combinations and some models in Figure 2a-c. To facilitate the comparison of multiple models, we use Spearman rank correlations ρ_s as a summary metric. A high rank correlation (close to 1) indicates that spatial variability in the forcing variable (e.g. precipitation) almost completely explains spatial variability in the output variable (e.g. groundwater recharge). This corresponds to a scatter plot with a tight relationship, as in Figure 2b for H08. A low rank correlation indicates that other factors also matter (e.g. model parameters, other input data). This corresponds to a scatter plot with a scattered relationship, as in Figure 2b for PCR-GLOBWB. It is important to note that a high correlation is not a measure of goodness of fit. The correlations simply characterize the strength of the relationship between forcing and response variables.

Besides comparing functional relationships between models, we compare the models to functional relationships based on several observational datasets and the semi-empirical equation introduced by Budyko (50), listed in Table 1.

Having found clear differences between major climate zones (Figure 1), we divide the world into four climatic regions (see Materials and Methods for details). Based on the aridity index (here defined as N/P), a place is categorized as either wet ($N/P < 1$) or dry ($N/P > 1$). Based on how many days per year fall below a 1°C temperature threshold, a place is categorized as either cold (more than one month below 1°C) or warm (less than one month below 1°C). This results in four categories: wet-warm (18% of modeled area), wet-cold (15%), dry-cold (24%), and dry-warm (43%), shown in Figure 2d.

Precipitation and evapotranspiration There are some differences in magnitude, but the ranking between the climate regions is the same for all models (Figure 3a and Table S3 in the Supporting Information). We find the strongest P-E_a-relationships in dry-warm places (ρ_s ranges from 0.90-0.98) and the weakest P-E_a-relationships in wet-warm places (ρ_s: 0.57-0.73). The Budyko equation (50) predicts higher correlations overall, but the same ranking. This reflects the fact that in dry (i.e. water-limited) places, precipitation primarily evaporates, while in wet (i.e. energy-limited) places, evapotranspiration is limited by the available energy. Contrary to the models and the Budyko equation, FLUXCOM data (51) show higher values for wet-cold than for dry-cold places (Figure 3a and Table 1).

Net radiation and evapotranspiration Most of the models show similar magnitudes and a similar ranking between the climate regions (Figure 3b and Table S3). We find the strongest N-E_a-relationships in wet-cold places (ρ_s: 0.56-0.96) and the weakest N-E_a-relationships in dry-cold places (ρ_s: 0.26-0.70). This agrees with the Budyko equation and reflects the fact that in wet (i.e. energy-limited) places, net radiation is the primary control on actual evapotranspiration, while in dry (i.e. water-limited) places, net radiation is a less strong control. There are, however, differences in the ranking for some of the models, especially for dry-warm places. For CWatM and WaterGAP2 dry-warm and not dry-cold places show the lowest correlation (0.12 and 0.41, respectively), and for MATSIRO dry-warm places show the highest correlation (0.70). FLUXCOM data show very high correlations for all regions (0.79-0.94; higher than most models), even for dry-cold regions (0.79), which show the lowest correlations in the models (0.26-0.70) and for Budyko (0.59) (Figure 3b and Table 1).

Precipitation and groundwater recharge The models show little agreement in their P-R-relationships (Figure 3c and Table S3). The largest variability is seen in dry-cold places (ρ_s: 0.35-0.84), followed closely by dry-warm (0.48-0.95) and wet-cold (0.47-0.90) places, while the lowest variability is seen in wet-warm places (0.70-0.88). CLM4.5, MATSIRO, WaterGAP2 and H08 show the highest correlations overall (0.71-0.95 across all climate regions), while other models (CWatM, JULES-W1, LPJmL, PCR-GLOBWB) show lower and more variable correlations (0.35-0.85). Some models show a clear difference between the climate regions (e.g. JULES-W1; ρ_s: 0.35-0.85), while others show little variability (e.g. MATSIRO; ρ_s: 0.76-0.88). Groundwater recharge observations for Africa (52) and the largest global scale groundwater recharge dataset compiled up to date (53) suggest high to very high correlations (0.74-0.84) in dry-warm places, which is similar to most models except for PCR-GLOBWB. Observations (53) suggest no correlation (-0.04) for wet-warm places and low correlation for

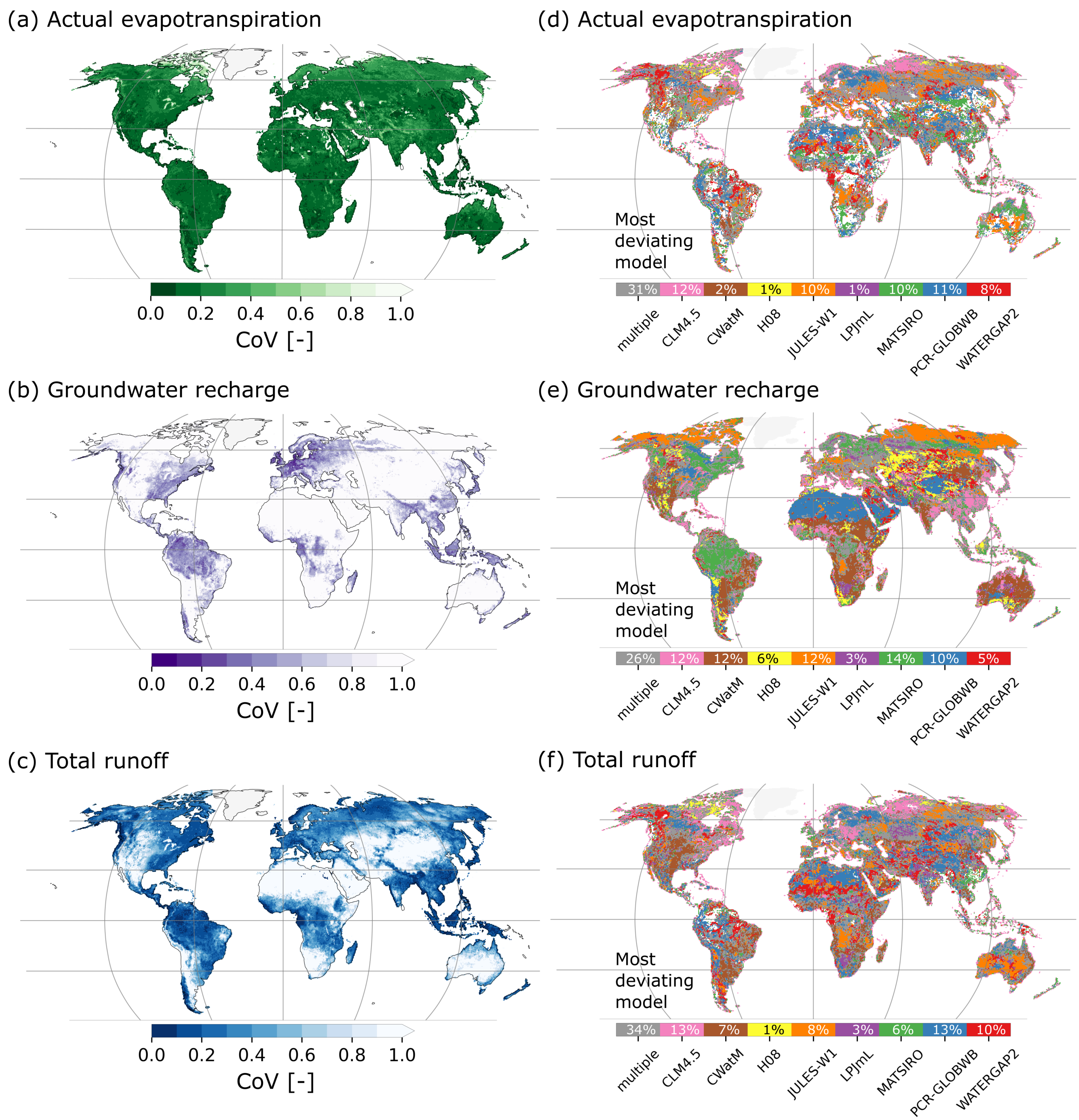

Fig. 1. Left: maps showing the coefficient of variation, calculated per grid cell as the standard deviation divided by the mean of the 8 models. for different water fluxes: actual evapotranspiration (a), groundwater recharge (b), and total runoff (c). Lighter areas ("white spaces"; see 36) indicate high CoV values and thus show where models disagree most. Right: maps showing which model deviates most from the ensemble mean for each grid cell and thus contributes the most to the CoV shown in (a)-(c) for different water fluxes: actual evapotranspiration (d), groundwater recharge (e), and total runoff (f). Dark gray areas in (d)-(f) indicate that multiple models deviate similarly strongly from the ensemble mean. Empty, white areas in (d)-(f) indicate that no model deviates strongly from the ensemble mean. The percentages shown in (d)-(f) refer to the fraction of grid cells (and not land area) covered by each model. Greenland is masked out for the analysis.

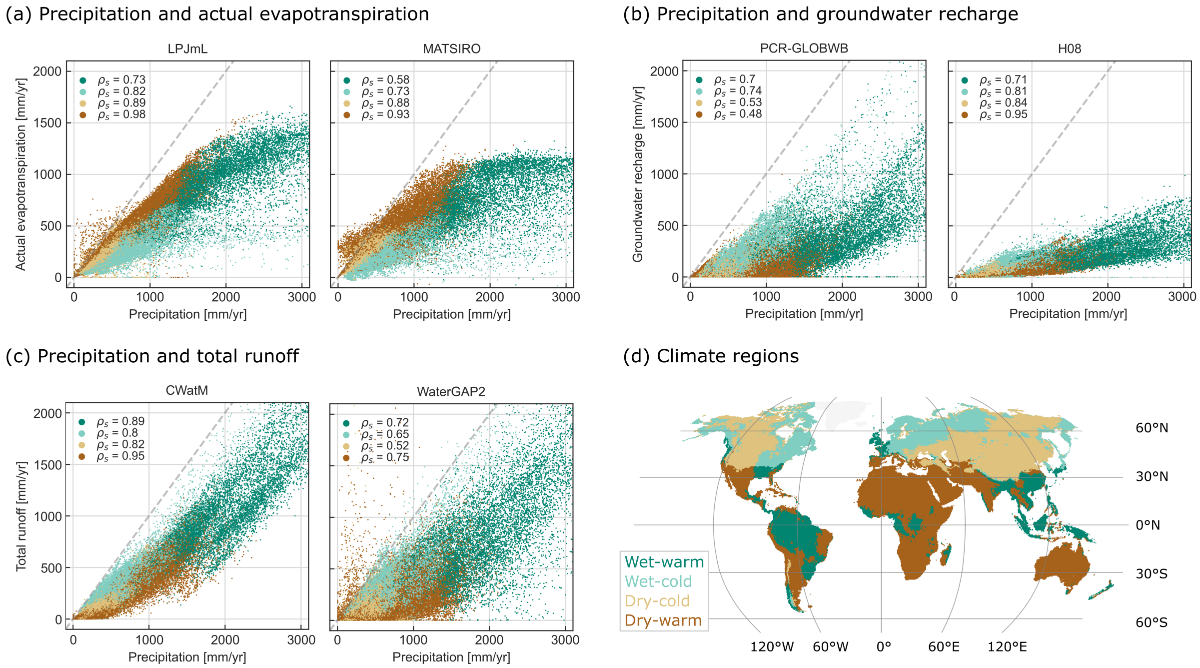

Fig. 2. Scatter plots that exemplary show functional relationships for selected models and variables. Due to space constraints, we focus on a few examples with differing relationships. Scatter plots for all variable pairs are shown in Figures S18-23 in the Supporting Information. Variables shown are (a) precipitation and actual evapotranspiration for LPJmL and MATSIRO, (b) precipitation and groundwater recharge for H08 and PCR-GLOBWB, and (c) precipitation and total runoff for WaterGAP2 and CWatM. Each dot represents one grid cell and is based on the 30-year average of each flux. Spearman rank correlations ρ_s measure the strength of the relationship between forcing and response variables and are calculated for all grid cells within a climate region. Dots are colored according to the regions shown in (d). The definition of the climate regions can be found in the Materials and Methods section. The dashed line shows the 1:1 line, indicating the water limit assuming all water is supplied by precipitation. Some models have grid cells that exceed this water limit, for instance due to water transfers from neighboring cells. Detailed model-specific explanations are given in the Supporting Information.

dry-cold places (0.28), which disagrees with all models (Figure 3c and Table 1).

Net radiation and groundwater recharge Most models show clear differences in magnitude and in ranking between the climate regions, but there is no common pattern in their N-R-relationships (Figure 3d and Table S3). We find the largest variability in dry-cold places (ρ_s: -0.35-0.51) and the lowest variability in wet-warm places (0.23-0.54). The mostly positive rank correlation between groundwater recharge and net radiation suggests that higher net radiation is associated with more groundwater recharge. This is counter-intuitive, but can be explained by the positive correlation between net radiation and precipitation (ρ_s: 0.48-0.77 for the four climate regions; see Figure S1 in the Supporting Information).

Precipitation and total runoff The models show mixed agreement in their P-Q-relationships (Figure 3e and Table S3). LPJmL, H08, and CWatM show very high correlations (0.77-0.95) for all climate regions, while WaterGAP2 and PCR-GLOBWB show the lowest correlations overall (0.52-0.75). Almost all models show higher correlations for warm places (0.71-0.95) than for cold places (0.52 to 0.82), so the primary distinction here is between warm and cold, and not between wet and dry as for evapotranspiration. This ranking agrees with the Budyko equation and GRUN (an observation-based global gridded runoff dataset; 54), but not with GSIM (data from the global streamflow and metadata archive; 55, 56). The Budyko equation predicts high correlations for all climate regions (0.87-0.99), while GSIM (0.73-0.89) and GRUN (0.28-0.93) show more variability and a different ranking between the climate regions. Most disagreement can be found in dry-cold places, both between models (ρ_s: 0.52-0.82) and between GRUN (0.28), GSIM (0.89) and Budyko (0.90) (Figure 3e and Table 1).

Net radiation and total runoff The ranking is mostly consistent and all models show rather large variability in their N-Q-relationships between the climate regions (Figure 3f and Table S3). Dry-cold places have low to negative correlations (-0.18-0.14), wet-warm and wet-cold places have low to medium correlations (0.16-0.50), and dry-warm places have the highest correlations overall (0.12-0.73). This tendency agrees with the Budyko equation (Figure 3f and Table 1). Similar to groundwater recharge, the mostly positive correlation between total runoff and net radiation suggests that higher net radiation is associated with more runoff, which can be explained by the positive correlation between net radiation and precipitation.

Discussion

To what extent do key water fluxes simulated by global water models disagree with each other, and how does the disagreement vary spatially?. Overall, we find the strongest model disagreement for groundwater recharge (mean grid cell CoV = 1.17), some disagreement for total runoff (mean grid cell CoV = 0.54), and the best agreement for evapotranspiration (mean grid cell CoV = 0.23). This is not unexpected, as groundwater recharge is arguably the least understood process (53, 58) and it is often represented in a rather simplified way in the models (59). Another reason might be that – averaged globally – actual evapotranspiration is the largest flux and

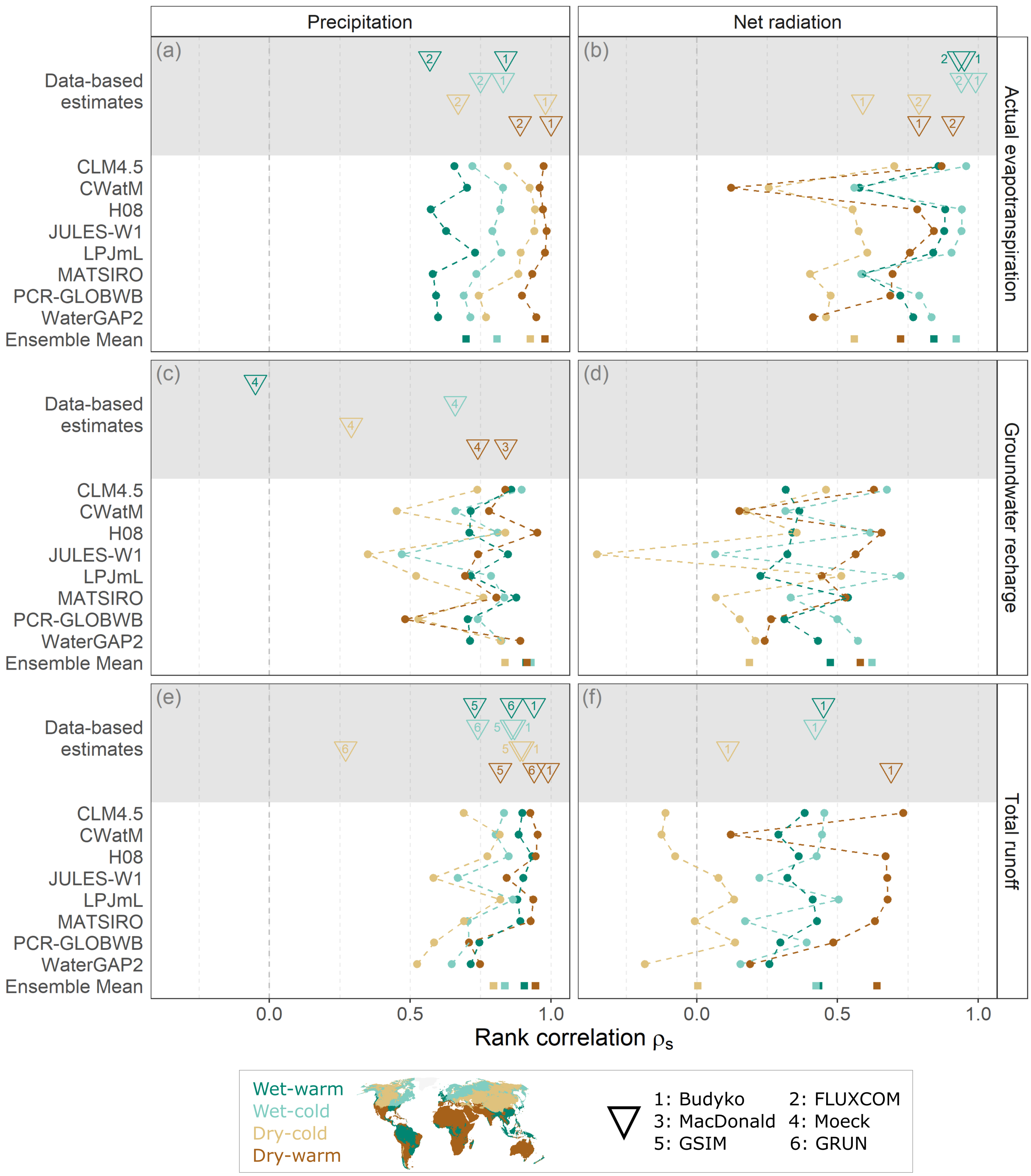

Fig. 3. Spearman rank correlations ρ_s between forcing variables (precipitation, net radiation) and water fluxes (actual evapotranspiration, groundwater recharge, and total runoff), divided into different climate regions. Net radiation for LPJmL and PCR-GLOBWB is not available and is estimated as the median of the other models (per grid cell). The lines connecting the dots are only there as a visual aid. The numbered triangles show observation-based rank correlations, with numbers indicating the corresponding data source (see Table 1). Observation-based rank correlations are only shown if they are based on more than 50 data points.

Table 1. Spearman rank correlations ρ_s between forcing variables and water fluxes and number of observations based on different observation-based datasets and the Budyko equation. The percentage of grid cells per climate region is given in brackets. The Budyko equation was forced per grid cell with the same forcing as the models (indicated by *), and thus covers approximately the same extent as the models (except for cells with negative net radiation). The gridded datasets (FLUXCOM, GRUN) are available at the same resolution as the models and thus also cover approximately the same extent (except for non-vegetated areas in the case of FLUXCOM). This is indicated by *m.e.* for model extent. For datasets without matching precipitation data, we used GSWP3 reanalysis data. *Number* corresponds to the numbers used in Figure 3. FLUXNET rank correlations and the MacDonald rank correlation for the wet-warm region are shown in brackets because of the very small sample sizes (50 or less); they are not shown in Figure 3. Dashes (-) indicate that correlations could not be calculated because no observations were available. Details can be found in the Materials and Methods section.

Water flux	Forcing	Source	Number	Wet-warm (15%)		Wet-cold (23%)		Dry-cold (28%)		Dry-warm (34%)	
				ρ_s	Count	ρ_s	Count	ρ_s	Count	ρ_s	Count
E_a	P	Budyko* (50)	1	0.84	m.e.	0.83	m.e.	0.98	m.e.	1.00	m.e.
E_a	P	FLUXCOM (51)	2	0.57	m.e.	0.75	m.e.	0.67	m.e.	0.89	m.e.
E_a	P	FLUXNET (57)	-	(0.72)	13	(0.36)	50	(0.57)	15	(0.51)	47
E_a	N	Budyko* (50)	1	0.95	m.e.	0.99	m.e.	0.59	m.e.	0.79	m.e.
E_a	N	FLUXCOM (51)	2	0.93	m.e.	0.94	m.e.	0.79	m.e.	0.91	m.e.
E_a	N	FLUXNET (57)	-	(0.67)	13	(0.42)	50	(0.72)	15	(0.41)	47
R	P	MacDonald (52)	3	(0.0)	4	-	0	-	0	0.84	130
R	P	Moeck (53)	4	-0.05	234	0.66	83	0.29	100	0.74	4772
Q	P	Budyko* (50)	1	0.94	m.e.	0.87	m.e.	0.90	m.e.	0.99	m.e.
Q	P	GSIM (55, 56)	5	0.73	1438	0.86	1255	0.89	593	0.82	1207
Q	P	GRUN (54)	6	0.86	m.e.	0.74	m.e.	0.27	m.e.	0.94	m.e.
Q	N	Budyko* (50)	1	0.45	m.e.	0.42	m.e.	0.11	m.e.	0.69	m.e.

thus its relative variability might be smaller than that of total runoff and especially groundwater recharge. The models disagree particularly in dry regions (e.g. Australia, outer-tropical Africa) and in cold regions (e.g. most of continental Asia and North America). This echoes existing literature (e.g. 1, 26, 60) and highlights the need for model refinement in dry and/or cold regions, which are under-researched and strongly affected by climate change (61, 62).

The disagreement between global water models underscores the importance of using a model ensemble to account for model uncertainty (6, 8, 10, 11, 24, 63). However, creating such an ensemble is not straightforward (64). The use of a simple ensemble mean for each grid cell leads to higher correlations overall, sometimes even higher than any individual model (e.g. Figure 3c for wet-warm and wet-cold regions). This is because averaging smooths out variability in the forcing-response relationships compared to individual models (see Figure S26). This finding challenges, in line with Zaherpour et al. (60), the notion that the (unweighted) ensemble mean leads to more robust model estimates. Assigning meaningful weights to models or removing models from the ensemble (1, 65) is also not straightforward. Since no model consistently deviates the most, and since the most deviating models differ between the three fluxes (see Figure 1d-f), model weights would have to vary spatially and for each flux. Without more in-depth analyses it is probably best to use the ensemble spread to capture a wide range of behaviors, while acknowledging that even the ensemble spread might not capture all epistemic uncertainties (66).

How do global water models translate forcing variables into key water fluxes, i.e. which functional relationships do they represent?. Our evaluation shows that models differ substantially in the way they translate forcing variables into key water fluxes (see Figure 3 and Table S3).

For precipitation and actual evapotranspiration, the models show the same ranking between climate regions and rather small differences in magnitude, indicating that actual evapotranspiration is strongly constrained by the available water for all models. We find more variability for net radiation and evapotranspiration, with CWatM and WaterGAP2 showing particularly low correlations for dry-warm regions (0.12 and 0.41, respectively), while all other models show much higher correlations (0.69-0.87). There is no obvious correspondence between the potential evapotranspiration scheme used (e.g. Priestley-Taylor for LPJmL and WaterGAP2, or Penman-Monteith for JULES-W1 and CWatM) and the rank correlations, implying that other factors also play an important role (see also 27, 63). It is worth noting that net radiation differs between models (Table S4), which adds uncertainty to this analysis but also highlights that the models already translate the same incoming total radiation differently into net radiation. This warrants a closer look in future studies, since a realistic depiction of the energy balance is important for climate change studies (67).

For precipitation and groundwater recharge, some models (CLM4.5, MATSIRO, WaterGAP2 and H08) show high to very high correlations (0.71-0.95) for all climate regions, suggesting that precipitation is the dominant control on groundwater recharge across all climate regions in these models. Other models (CWatM, JULES-W1, LPJmL, PCR-GLOBWB) show much lower and more variable correlations (0.35-0.85), suggesting different controls on groundwater recharge (e.g. model structural decisions and parameterizations). This difference can also be seen in Figure 2b, where H08 has a much tighter P-R-relationship than PCR-GLOBWB. H08 and WaterGAP2 use the same approach to calculate recharge (59) and they show almost the same rank correlations, indicating that the functional relationships might be relatable to the model structure in this case. We find high variability, and mostly positive correlations, for net radiation and groundwater recharge. The models probably produce more groundwater recharge in regions with higher net radiation because precipitation is also higher in these regions. While it is difficult to interpret these correlations, the large variability still suggests considerable differences between models.

For precipitation and total runoff, WaterGAP2 and PCR-GLOBWB both show lower correlations (0.52 to 0.75) than most other models (0.77 to 0.95 for CLM4.5, CWatM, H08, LPJmL, and MATSIRO). This suggests clear differences in how strongly total runoff is controlled by precipitation and in how these models generate runoff, echoing Bierkens (68), who highlighted runoff generation as main area for model improvement. This difference can also be seen in Figure 2c, where CWatM shows a much tighter P-Q-relationship than WaterGAP2. WaterGAP2 is the only model here that is calibrated against streamflow observations (59), which might explain why it shows the lowest rank correlations for total runoff. For total runoff, it is challenging to relate model structure to functional behavior, since it consists of different runoff components. Analyzing the different runoff components individually might shed more light on how different process conceptualizations (e.g. dependence of surface runoff on antecedent wetness) affect model behavior. Similar to groundwater recharge, we find mostly positive correlations for net radiation and total runoff, probably because precipitation is higher in regions with higher net radiation.

While rank correlations expose clear differences between models, our approach here should be seen as a first step in quantifying functional relationships. Rank correlations only measure how strongly two variables are related to each other and they only capture uni-directional dependencies. Hence they cannot capture all the possible differences (e.g. differences in average flux magnitudes, visible in Figure 2 and quantified in Table S4 in the Supplementary Information). For example, since precipitation and net radiation are correlated, we should not conclude that higher net radiation causes more groundwater recharge or runoff. More generally, rank correlations themselves cannot always be easily explained by underlying mechanisms. Future studies should aim at getting a better mechanistic understanding of the patterns found here and explore additional ways to quantify functional relationships, including the use of machine learning methods.

Can we use data and existing knowledge to derive functional relationships and use them to constrain expected model behavior?. The Budyko equation (50) assumes complete dependence on aridity (here defined as N/P) and likely presents an upper limit in terms of correlations. It should thus be seen as a useful comparison, but not as the "correct" model, given that different studies have shown that climate seasonality (69), vegetation type (70), snow (71), and inter-catchment groundwater flow (72) can affect the long-term water balance beyond aridity. Models and data reflect water- and energy-limited conditions, but tend to show lower correlations than the Budyko equation (Figure 3). An exception are dry-cold regions, for which FLUXCOM data show a stronger N-E_a-relationship and a weaker P-E_a-relationship. This might be due to a poor representation of energy balance processes in cold places by the Budyko equation (73) and in current models (67).

The Budyko framework also assumes that long-term runoff only depends on aridity. Consequently, we find higher correlations for the Budyko equation than for both datasets and most of the models. We again find large differences in dry-cold regions (see also 1), where GRUN shows a much weaker P-Q-relationship than the models and GSIM.

Recent studies have shown a strong influence of precipitation and aridity on groundwater recharge (52, 53). While our results also suggest that precipitation is an important control on groundwater recharge, they show that models tend to overestimate the strength of that control, especially in wet-warm regions and to a lesser extent in dry-cold regions. Perceptual models of groundwater recharge generation usually include climate, but also soil characteristics, topography, and land use (74). Recently, Cuthbert et al. (75) found that local hydrogeology influences P-R-relationships in Africa, though this is difficult to generalize to larger regions given limitations in global datasets (25). In line with those findings, our results strongly suggest that models overestimate the degree to which climate forcing variables control groundwater recharge.

We have collected several observational or observation-driven datasets to derive empirical forcing-response relationships, but there remain some challenges. Observation-based estimates contain uncertainty, inherited from the observational datasets themselves and due to small numbers of observations in certain regions. Since not all datasets come with corresponding forcing and response variables, we sometimes had to pair observations with other forcing datasets, which can introduce additional uncertainty (see Materials and Methods for an extended discussion). Looking ahead, the gaps in the observation-based correlations shown in Table 1 are a first step to identify regions and variables where more measurements would be especially useful to constrain expected functional relationships. In addition, more quality-controlled datasets with uncertainty estimates (e.g 52) are critical to obtain realistic uncertainty estimates for functional relationships. This would ultimately allow us to obtain robust ranges of functional behavior which we can benchmark our models against.

A global perspective for global models. Using functional relationships shifts the focus away from evaluating model performance in specific locations and from matching historical records to a more diagnostic and process-oriented evaluation of model behavior (76). Functional relationships allow us to focus on larger-scale assessments and to explore if dominant controls in the models are consistent with observations, theory and expectations, i.e. our perceptual model (36). This is critical for ensuring that models faithfully represent real-world systems, leading to more credible projections of environmental change impacts.

An advantage of functional relationships is that they relate different locations to each other, and thus take information out of its location-specific context and put it to a more large-scale use. However, the uneven distribution of observations poses challenges if we want to derive robust relationships. For example, recharge measurements have almost entirely been made in warm dry regions (97% of MacDonald et al. (52) and 92% of Moeck et al. (53)). Streamflow measurements have been made more frequently in wet regions (60% of the GSIM data (55, 56) used here) and globally, there is a placement bias of stream gauges towards wet regions (77), even though – according to our classification – short of two-thirds of the global land area are dry. While there are clear reasons for this spatial bias, we will have to explore how this bias affects functional relationships and how to most effectively enlarge our observational database.

In this study, we have focused on rank correlations between long-term averages of two forcing variables and three water fluxes, but this approach can easily be extended. Other variables, including state variables or stores (e.g. soil moisture, terrestrial water storage), possibly investigated at different time scales (e.g. monthly), should yield additional insights. There are existing metrics such as elasticities (34) that lend themselves for such an analysis, and there is room for new methods to be developed (e.g. characterizing thresholds in forcing-response relationships). Expanding our range of functional relationships, constrained by various observational datasets and expert knowledge, might eventually give us a knowledge base of realistic system behavior that can be used to evaluate models and diagnose model deficiencies, comparable to the use of emergent constraints in climate modeling (78).

More generally, functional relationships invite us to think about how the global water cycle functions, what we know, what we do not know, and what that means for a future under climate change (36). Our results here suggest that improved process understanding will be particularly important for energy balance processes, recharge processes, and generally in dry and/or cold regions. So how can we improve our process understanding? In 1986, Eagleson (79) stated that "science advances on two legs, analysis and experimentation, and at any moment one is ahead of the other. At the present time advances in hydrology appear to be data limited". For some processes, this still seems to be the case. But clearly, we have a wealth of data available and might ask ourselves: are we extracting enough information from the observations we have? Are there hydrological regularities yet to be found (80)? Even if the search for such regularities is challenging, it might be a fruitful and exciting endeavor for global hydrology.

Materials and Methods

Model data retrieval and processing. We analyzed 30-year (climatological) averages (1975-2004) from 8 global water models (49): CLM4.5 (41), CWatM (42), H08 (43), JULES-W1 (44), LPJmL (45), MATSIRO (46), PCR-GLOBWB (47), and WaterGAP2 (48). The model simulations were carried out following the ISIMIP 2b protocol and here we used model outputs forced with the Earth system model HadGEM2-ES under historical conditions (historical climate and CO_2 concentrations). We used precipitation P (ISIMIP variable name *pr*), net radiation N, actual evapotranspiration E_a (ISIMIP variable name *evap*), groundwater recharge R (ISIMIP variable name *qr*) and total runoff Q (ISIMIP variable name *qtot*). Note that Q here refers to runoff generated on the land fractions (and not surface water bodies) of each grid cell and does not include upstream inflows, which allows for comparison to grid cell P. P, E_a, R, and Q were downloaded from https://data.isimip.org/. Net radiation N is not an official ISIMIP output and was provided by the individual modeling groups. It is not available for all models, so we used the ensemble mean per grid cell for models without N data. We converted all fluxes to mm/y and removed E_a values larger than 10000 mm/y and set R values smaller than 0 to 0. A more detailed description is given in the Supporting Information.

CoV and most deviating model maps. For each grid cell, we calculated the coefficient of variation (CoV) by dividing the standard deviation by the mean using the 8 model outputs. Maps of the standard deviation are shown in the Supporting Information (Figures S5-7). To see which model dominates the ensemble spread, we checked for each grid cell which model shows the largest absolute difference (denoted by d_1) from the ensemble mean (denoted by μ). To see if multiple models dominate the ensemble spread, we also checked for each grid cell which model shows the second largest absolute difference (denoted by d_2) from the ensemble mean. If the relative difference between the largest and the second largest difference is less than 20%, i.e. $(d_1 - d_2)/d_1 < 0.2$, the grid cell falls into the category "multiple". If the relative difference between the most deviating model and the ensemble mean is less than 20%, i.e. $d_1/\mu < 0.2$, the grid cell is counted as having no most deviating model (empty areas on Figure 1d-f).

Functional relationships. As a metric for the strength of the functional relationships between model inputs and outputs, we use Spearman rank correlations ρ_s for each climate region. The Spearman rank correlation is a measure of the monotonicity between two variables and it is robust to outliers. We use the following categories for correlations: negative (<0), no to low correlation (0 to 0.25), medium correlation (0.25-0.5), high correlation (0.5-0.75), very high correlation (0.75-1.0).

Climate regions Based on the aridity index (here defined as N/P), a place is categorized as either wet ($N/P < 1$) or dry ($N/P > 1$). Note that we used the ensemble median for N. Based on how many days per year fall below a 1°C temperature threshold, a place is categorized as either cold (more than one month below 1°C) or warm (less than one month below 1°C). This results in four categories: wet-warm (15% of model grid cells / 18% of modeled area), wet-cold (23% / 15%), dry-cold (28% / 24%), and dry-warm (34% / 43%). To test how different decisions affect our climate region classification, we also used the ensemble median of potential evapotranspiration E_p (partially downloaded, partially provided by the modeling groups) to calculate the aridity index (E_p/P), and we used a different threshold for our warm/cold distinction. This resulted in little differences overall, as can be seen in the Supporting Information (Figure S16).

Observational datasets and theory. For E_a, we used FLUXCOM data (51) (RS monthly 0.5° from 2001-2015) paired with GSWP3 P data (81) (downloaded from https://data.isimip.org/), and FLUXNET data (57) which include matching P data. For R, we used data from MacDonald et al. (52) which include matching P data, and data from Moeck et al. (53) paired with GSWP3 P data (81). For Q, we used GRUN data (54) from 1985-2004 paired with GSWP3 P data (81), and GSIM data (55, 56) from catchments with areas from 250-25000 km^2 with minimum 10y of data to ensure a sufficient number of catchments that do not differ too much in size from the model grid cells. We paired GSIM data with catchment-averaged MSWEP P data (82), which were calculated by Stein et al. (83).

To obtain theory-based estimates for E_a and Q, we forced the Budyko (50) equation (Eq.1) with HadGEM2-ES P and ensemble median N from the ISIMIP 2b models analyzed here.

$$\frac{E_a}{P} = \sqrt{\frac{N}{P}\tanh\left(\frac{P}{N}\right)\left(1-\exp\left(-\frac{N}{P}\right)\right)} \qquad [1]$$

More details on data processing and quality checks can be found in the Supporting Information.

Extended discussion on model forcing and scenario uncertainty. The choice of forcing product and differences in the treatment of human influences (e.g. water use and dams) might affect the functional relationships exhibited by the models. To get an idea how much uncertainty this introduces, we calculated correlations using WATCH-WFDEI forcing with either variable historical conditions (varsoc) or no human influences (nosoc) for WaterGAP2 and PCR-GLOBWB, carried out following the ISIMIP 2a protocol. The results, shown in the Supporting Information, stay essentially the same, suggesting that the model-based correlations are robust signatures of model behavior.

Extended discussion on data uncertainty. Since not all datasets come with matching P data, we sometimes paired the observations with GSWP3 reanalysis data (81). To get an idea how much uncertainty this introduces, we calculated rank correlations using different P data sources. Correlations calculated using the MacDonald et al. (52) R data with either GSWP3 P data or the accompanying P data are very similar for dry-warm places (0.83 and 0.84; see Supporting

Information). Using HadGEM2-ES P (the model forcing) data instead of GSWP3 P data to calculate correlations with FLUXCOM E_a (51), Moeck R (53), and GRUN Q (54), respectively, results in virtually no differences (results are shown in the Supporting information). This indicates that the correlations are robust, likely because rank correlations remain stable as long as relative differences between forcing values per grid cell stay the same.

Code and data availability. Model outputs can be accessed via the ISIMIP website (https://www.isimip.org/). Observational datasets can be accessed via the references shown in Table 1. Multi-annual averages and rank correlations will be uploaded to a repository and code can be found at https://github.com/HydroSysPotsdam/Global_model_evaluation (DOI for both will be created upon acceptance).

ACKNOWLEDGMENTS. SJG, RR, LS, and TW acknowledge support from the Alexander von Humboldt Foundation in the framework of the Alexander von Humboldt Professorship endowed by the German Federal Ministry of Education and Research (BMBF). This publication is based upon work from COST Action CA19139 – PROCLIAS, supported by COST (European Cooperation in Science and Technology, https://www.cost.eu). We thank Anneke Tombrägel for help with processing the FLUXNET data and Petra Döll for providing helpful comments on the manuscript. We also thank the ISIMIP team for their continued efforts within the ISIMIP project.

1. A Gädeke, et al., Performance evaluation of global hydrological models in six large Pan-Arctic watersheds. *Clim. Chang.* **163**, 1329–1351 (2020).
2. D Gerten, et al., Asynchronous exposure to global warming: freshwater resources and terrestrial ecosystems. *Environ. Res. Lett.* **8**, 034032 (2013) Publisher: IOP Publishing.
3. NW Arnell, SN Gosling, The impacts of climate change on river flood risk at the global scale. *Clim. Chang.* **134**, 387–401 (2016).
4. P Greve, et al., Global assessment of water challenges under uncertainty in water scarcity projections. *Nat. Sustain.* **1**, 486–494 (2018) Number: 9 Publisher: Nature Publishing Group.
5. J Schewe, et al., State-of-the-art global models underestimate impacts from climate extremes. *Nat. Commun.* **10**, 1005 (2019) Number: 1 Publisher: Nature Publishing Group.
6. W Thiery, et al., Intergenerational inequities in exposure to climate extremes. *Science* **374**, 158–160 (2021) Publisher: American Association for the Advancement of Science.
7. IPCC, *Climate Change 2022: Impacts, Adaptation, and Vulnerability. Contribution of Working Group II to the Sixth Assessment Report of the Intergovernmental Panel on Climate Change [H.-O. Pörtner, D.C. Roberts, M. Tignor, E.S. Poloczanska, K. Mintenbeck, A. Alegría, M. Craig, S. Langsdorf, S. Löschke, V. Möller, A. Okem, B. Rama (eds.)]*. (Cambridge University Press), (2022).
8. J Schewe, et al., Multimodel assessment of water scarcity under climate change. *Proc. Natl. Acad. Sci.* **111**, 3245–3250 (2014) Publisher: Proceedings of the National Academy of Sciences.
9. L Gudmundsson, et al., Globally observed trends in mean and extreme river flow attributed to climate change. *Science* **371**, 1159–1162 (2021) Publisher: American Association for the Advancement of Science.
10. Y Pokhrel, et al., Global terrestrial water storage and drought severity under climate change. *Nat. Clim. Chang.* **11**, 226–233 (2021) Number: 3 Publisher: Nature Publishing Group.
11. R Reinecke, et al., Uncertainty of simulated groundwater recharge at different global warming levels: a global-scale multi-model ensemble study. *Hydrol. Earth Syst. Sci.* **25**, 787–810 (2021) Publisher: Copernicus GmbH.
12. IGRAC, Global Groundwater Information System (2022) Published: ggis.un-igrac.org.
13. RW Hofste, et al., Aqueduct 3.0: Updated decision-relevant global water risk indicators. *World Resour. Inst.* pp. 1–53 (2019) Publisher: World Resources Institute.
14. J Sheffield, et al., A Drought Monitoring and Forecasting System for Sub-Sahara African Water Resources and Food Security. *Bull. Am. Meteorol. Soc.* **95**, 861–882 (2014) Publisher: American Meteorological Society Section: Bulletin of the American Meteorological Society.
15. P Döll, K Fiedler, Global-scale modeling of groundwater recharge. *Hydrol. Earth Syst. Sci.* **12**, 863–885 (2008) Publisher: Copernicus GmbH.
16. Y Wada, et al., Global depletion of groundwater resources. *Geophys. Res. Lett.* **37** (2010) _eprint: https://onlinelibrary.wiley.com/doi/pdf/10.1029/2010GL044571.
17. AS Richey, et al., Quantifying renewable groundwater stress with GRACE. *Water Resour. Res.* **51**, 5217–5238 (2015) _eprint: https://onlinelibrary.wiley.com/doi/pdf/10.1002/2015WR017349.
18. IEM de Graaf, et al., A global-scale two-layer transient groundwater model: Development and application to groundwater depletion. *Adv. Water Resour.* **102**, 53–67 (2017).
19. R Reinecke, et al., Challenges in developing a global gradient-based groundwater model (G^3M v1.0) for the integration into a global hydrological model. *Geosci. Model. Dev.* **12**, 2401–2418 (2019) Publisher: Copernicus GmbH.
20. R Dankers, et al., First look at changes in flood hazard in the Inter-Sectoral Impact Model Intercomparison Project ensemble. *Proc. Natl. Acad. Sci.* **111**, 3257–3261 (2014) Publisher: Proceedings of the National Academy of Sciences.
21. L Samaniego, et al., Anthropogenic warming exacerbates European soil moisture droughts. *Nat. Clim. Chang.* **8**, 421–426 (2018) Number: 5 Publisher: Nature Publishing Group.
22. C Prudhomme, et al., Hydrological droughts in the 21st century, hotspots and uncertainties from a global multimodel ensemble experiment. *Proc. Natl. Acad. Sci.* **111**, 3262–3267 (2014) Publisher: Proceedings of the National Academy of Sciences.
23. HE Beck, et al., Global evaluation of runoff from 10 state-of-the-art hydrological models. *Hydrol. Earth Syst. Sci.* **21**, 2881–2903 (2017) Publisher: Copernicus GmbH.
24. BR Scanlon, et al., Global models underestimate large decadal declining and rising water storage trends relative to GRACE satellite data. *Proc. Natl. Acad. Sci.* **115**, E1080–E1089 (2018) Publisher: Proceedings of the National Academy of Sciences.
25. C West, et al., Ground truthing global-scale model estimates of groundwater recharge across Africa. *Sci. The Total. Environ.* **858**, 159765 (2023).
26. I Giuntoli, JP Vidal, C Prudhomme, DM Hannah, Future hydrological extremes: the uncertainty from multiple global climate and global hydrological models. *Earth Syst. Dyn.* **6**, 267–285 (2015) Publisher: Copernicus GmbH.
27. R Wartenburger, et al., Evapotranspiration simulations in ISIMIP2a—Evaluation of spatio-temporal characteristics with a comprehensive ensemble of independent datasets. *Environ. Res. Lett.* **13**, 075001 (2018) Publisher: IOP Publishing.
28. A Hartmann, T Gleeson, Y Wada, T Wagener, Enhanced groundwater recharge rates and altered recharge sensitivity to climate variability through subsurface heterogeneity. *Proc. Natl. Acad. Sci.* **114**, 2842–2847 (2017) Publisher: Proceedings of the National Academy of Sciences.
29. T Gleeson, et al., GMD perspective: The quest to improve the evaluation of groundwater representation in continental- to global-scale models. *Geosci. Model. Dev.* **14**, 7545–7571 (2021) Publisher: Copernicus GmbH.
30. T Wagener, R Reinecke, F Pianosi, On the evaluation of climate change impact models. *WIREs Clim. Chang.* **13**, e772 (2022) _eprint: https://onlinelibrary.wiley.com/doi/pdf/10.1002/wcc.772.
31. RD Koster, P Milly, The Interplay between Transpiration and Runoff Formulations in Land Surface Schemes Used with Atmospheric Models. *J. Clim.* **10** (1997).
32. R Knutti, MAA Rugenstein, GC Hegerl, Beyond equilibrium climate sensitivity. *Nat. Geosci.* **10**, 727–736 (2017) Number: 10 Publisher: Nature Publishing Group.
33. J NĚMEC, J SCHAAKE, Sensitivity of water resource systems to climate variation. *Hydrol. Sci. J.* **27**, 327–343 (1982) Publisher: Taylor & Francis _eprint: https://doi.org/10.1080/02626668209491113.
34. A Sankarasubramanian, RM Vogel, JF Limbrunner, Climate elasticity of streamflow in the United States. *Water Resour. Res.* **37**, 1771–1781 (2001) _eprint: https://onlinelibrary.wiley.com/doi/pdf/10.1029/2000WR900330.
35. B Nijssen, GM O'Donnell, AF Hamlet, DP Lettenmaier, Hydrologic Sensitivity of Global Rivers to Climate Change. *Clim. Chang.* **50**, 143–175 (2001).
36. T Wagener, et al., On doing hydrology with dragons: Realizing the value of perceptual models and knowledge accumulation. *WIREs Water* **8**, e1550 (2021) _eprint: https://onlinelibrary.wiley.com/doi/pdf/10.1002/wat2.1550.
37. RM Vogel, A Sankarasubramanian, Validation of a watershed model without calibration. *Water Resour. Res.* **39** (2003) _eprint: https://onlinelibrary.wiley.com/doi/pdf/10.1029/2002WR001940.
38. E Kapangaziwiri, D Hughes, T Wagener, Incorporating uncertainty in hydrological predictions for gauged and ungauged basins in southern Africa. *Hydrol. Sci. J.* **57**, 1000–1019 (2012) Publisher: Taylor & Francis _eprint: https://doi.org/10.1080/02626667.2012.690881.
39. TJ Troy, EF Wood, J Sheffield, An efficient calibration method for continental-scale land surface modeling. *Water Resour. Res.* **44** (2008) _eprint: https://onlinelibrary.wiley.com/doi/pdf/10.1029/2007WR006513.
40. P Greve, P Burek, Y Wada, Using the Budyko Framework for Calibrating a Global Hydrological Model. *Water Resour. Res.* **56**, e2019WR026280 (2020) _eprint: https://onlinelibrary.wiley.com/doi/pdf/10.1029/2019WR026280.
41. W Thiery, et al., Present-day irrigation mitigates heat extremes. *J. Geophys. Res. Atmospheres* **122**, 1403–1422 (2017) _eprint: https://onlinelibrary.wiley.com/doi/pdf/10.1002/2016JD025740.
42. P Burek, et al., Development of the Community Water Model (CWatM v1.04) – a high-resolution hydrological model for global and regional assessment of integrated water resources management. *Geosci. Model. Dev.* **13**, 3267–3298 (2020) Publisher: Copernicus GmbH.
43. N Hanasaki, S Yoshikawa, Y Pokhrel, S Kanae, A global hydrological simulation to specify the sources of water used by humans. *Hydrol. Earth Syst. Sci.* **22**, 789–817 (2018) Publisher: Copernicus GmbH.
44. MJ Best, et al., The Joint UK Land Environment Simulator (JULES), model description – Part 1: Energy and water fluxes. *Geosci. Model. Dev.* **4**, 677–699 (2011) Publisher: Copernicus GmbH.
45. J Jägermeyr, et al., Water savings potentials of irrigation systems: global simulation of processes and linkages. *Hydrol. Earth Syst. Sci.* **19**, 3073–3091 (2015) Publisher: Copernicus GmbH.
46. K Takata, S Emori, T Watanabe, Development of the minimal advanced treatments of surface interaction and runoff. *Glob. Planet. Chang.* **38**, 209–222 (2003).
47. EH Sutanudjaja, et al., PCR-GLOBWB 2: a 5 arcmin global hydrological and water resources model. *Geosci. Model. Dev.* **11**, 2429–2453 (2018) Publisher: Copernicus GmbH.
48. H Müller Schmied, et al., Variations of global and continental water balance components as impacted by climate forcing uncertainty and human water use. *Hydrol. Earth Syst. Sci.* **20**, 2877–2898 (2016) Publisher: Copernicus GmbH.
49. K Frieler, et al., Assessing the impacts of 1.5 °C global warming – simulation protocol of the Inter-Sectoral Impact Model Intercomparison Project (ISIMIP2b). *Geosci. Model. Dev.* **10**, 4321–4345 (2017) Publisher: Copernicus GmbH.
50. MI Budyko, Climate and life, (Academic Press), Technical Report 18 (1974).
51. M Jung, et al., The FLUXCOM ensemble of global land-atmosphere energy fluxes. *Sci. Data* **6**, 74 (2019) Number: 1 Publisher: Nature Publishing Group.
52. AM MacDonald, et al., Mapping groundwater recharge in Africa from ground observations and implications for water security. *Environ. Res. Lett.* **16**, 034012 (2021) Publisher: IOP Publishing.
53. C Moeck, et al., A global-scale dataset of direct natural groundwater recharge rates: A review of variables, processes and relationships. *Sci. The Total. Environ.* **717**, 137042 (2020).

54. G Ghiggi, V Humphrey, SI Seneviratne, L Gudmundsson, GRUN: an observation-based global gridded runoff dataset from 1902 to 2014. *Earth Syst. Sci. Data* **11**, 1655–1674 (2019) Publisher: Copernicus GmbH.
55. HX Do, L Gudmundsson, M Leonard, S Westra, The Global Streamflow Indices and Metadata Archive (GSIM) – Part 1: The production of a daily streamflow archive and metadata. *Earth Syst. Sci. Data* **10**, 765–785 (2018) Publisher: Copernicus GmbH.
56. L Gudmundsson, HX Do, M Leonard, S Westra, The Global Streamflow Indices and Metadata Archive (GSIM) – Part 2: Quality control, time-series indices and homogeneity assessment. *Earth Syst. Sci. Data* **10**, 787–804 (2018) Publisher: Copernicus GmbH.
57. G Pastorello, et al., The FLUXNET2015 dataset and the ONEFlux processing pipeline for eddy covariance data. *Sci. Data* **7**, 225 (2020) Number: 1 Publisher: Nature Publishing Group.
58. TR Green, et al., Beneath the surface of global change: Impacts of climate change on groundwater. *J. Hydrol.* **405**, 532–560 (2011).
59. CE Telteu, et al., Understanding each other's models: an introduction and a standard representation of 16 global water models to support intercomparison, improvement, and communication. *Geosci. Model. Dev.* **14**, 3843–3878 (2021) Publisher: Copernicus GmbH.
60. J Zaherpour, et al., Worldwide evaluation of mean and extreme runoff from six global-scale hydrological models that account for human impacts. *Environ. Res. Lett.* **13**, 065015 (2018) Publisher: IOP Publishing.
61. F Felfelani, Y Wada, L Longuevergne, YN Pokhrel, Natural and human-induced terrestrial water storage change: A global analysis using hydrological models and GRACE. *J. Hydrol.* **553**, 105–118 (2017).
62. D Zoccatelli, et al., Contrasting rainfall-runoff characteristics of floods in desert and Mediterranean basins. *Hydrol. Earth Syst. Sci.* **23**, 2665–2678 (2019) Publisher: Copernicus GmbH.
63. I Haddeland, et al., Multimodel Estimate of the Global Terrestrial Water Balance: Setup and First Results. *J. Hydrometeorol.* **12**, 869–884 (2011) Publisher: American Meteorological Society Section: Journal of Hydrometeorology.
64. J Rougier, Ensemble Averaging and Mean Squared Error. *J. Clim.* **29**, 8865–8870 (2016) Publisher: American Meteorological Society Section: Journal of Climate.
65. NP Gillett, Weighting climate model projections using observational constraints. *Philos. Transactions Royal Soc. A: Math. Phys. Eng. Sci.* **373**, 20140425 (2015) Publisher: Royal Society.
66. KJ Beven, et al., Epistemic uncertainties and natural hazard risk assessment – Part 2: What should constitute good practice? *Nat. Hazards Earth Syst. Sci.* **18**, 2769–2783 (2018) Publisher: Copernicus GmbH.
67. PCD Milly, KA Dunne, Colorado River flow dwindles as warming-driven loss of reflective snow energizes evaporation. *Science* **367**, 1252–1255 (2020) Publisher: American Association for the Advancement of Science.
68. MFP Bierkens, Global hydrology 2015: State, trends, and directions. *Water Resour. Res.* **51**, 4923–4947 (2015) _eprint: https://onlinelibrary.wiley.com/doi/pdf/10.1002/2015WR017173.
69. PCD Milly, Climate, soil water storage, and the average annual water balance. *Water Resour. Res.* **30**, 2143–2156 (1994) _eprint: https://onlinelibrary.wiley.com/doi/pdf/10.1029/94WR00586.
70. L Zhang, WR Dawes, GR Walker, Response of mean annual evapotranspiration to vegetation changes at catchment scale. *Water Resour. Res.* **37**, 701–708 (2001) _eprint: https://onlinelibrary.wiley.com/doi/pdf/10.1029/2000WR900325.
71. WR Berghuijs, RA Woods, M Hrachowitz, A precipitation shift from snow towards rain leads to a decrease in streamflow. *Nat. Clim. Chang.* **4**, 583–586 (2014) Number: 7 Publisher: Nature Publishing Group.
72. Y Liu, T Wagener, HE Beck, A Hartmann, What is the hydrologically effective area of a catchment? *Environ. Res. Lett.* **15**, 104024 (2020) Publisher: IOP Publishing.
73. AA Meira Neto, GY Niu, T Roy, S Tyler, PA Troch, Interactions between snow cover and evaporation lead to higher sensitivity of streamflow to temperature. *Commun. Earth & Environ.* **1**, 1–7 (2020) Number: 1 Publisher: Nature Publishing Group.
74. BR Scanlon, RW Healy, PG Cook, Choosing appropriate techniques for quantifying groundwater recharge. *Hydrogeol. J.* p. 22 (2002).
75. MO Cuthbert, et al., Observed controls on resilience of groundwater to climate variability in sub-Saharan Africa. *Nature* **572**, 230–234 (2019) Number: 7768 Publisher: Nature Publishing Group.
76. HV Gupta, T Wagener, Y Liu, Reconciling theory with observations: elements of a diagnostic approach to model evaluation. *Hydrol. Process.* **22**, 3802–3813 (2008) _eprint: https://onlinelibrary.wiley.com/doi/pdf/10.1002/hyp.6989.
77. CA Krabbenhoft, et al., Assessing placement bias of the global river gauge network. *Nat. Sustain.* pp. 1–7 (2022) Publisher: Nature Publishing Group.
78. V Eyring, et al., Taking climate model evaluation to the next level. *Nat. Clim. Chang.* **9**, 102–110 (2019) Number: 2 Publisher: Nature Publishing Group.
79. PS Eagleson, The emergence of global-scale hydrology. *Water Resour. Res.* **22**, 6S–14S (1986) _eprint: https://onlinelibrary.wiley.com/doi/pdf/10.1029/WR022i09Sp0006S.
80. JCI Dooge, Looking for hydrologic laws. *Water Resour. Res.* **22**, 46S–58S (1986) _eprint: https://onlinelibrary.wiley.com/doi/pdf/10.1029/WR022i09Sp0046S.
81. PA Dirmeyer, et al., GSWP-2: Multimodel Analysis and Implications for Our Perception of the Land Surface. *Bull. Am. Meteorol. Soc.* **87**, 1381–1398 (2006) Publisher: American Meteorological Society Section: Bulletin of the American Meteorological Society.
82. HE Beck, et al., MSWEP V2 Global 3-Hourly 0.1° Precipitation: Methodology and Quantitative Assessment. *Bull. Am. Meteorol. Soc.* **100**, 473–500 (2019) Publisher: American Meteorological Society Section: Bulletin of the American Meteorological Society.
83. L Stein, F Pianosi, R Woods, Event-based classification for global study of river flood generating processes. *Hydrol. Process.* **34**, 1514–1529 (2020) _eprint: https://onlinelibrary.wiley.com/doi/pdf/10.1002/hyp.13678.